# HYDRAULIC RAM STUDIES

Wesley Richard Soper

Naval Postgraduate School
Monterey, California

December 1973

SECURITY CLASSIFICATION OF THIS PAGE (When Data Entered)

## REPORT DOCUMENTATION PAGE

READ INSTRUCTIONS BEFORE COMPLETING FORM

| | |
|---|---|
| 1. REPORT NUMBER | 2. GOVT ACCESSION NO. / 3. RECIPIENT'S CATALOG NUMBER |
| 4. TITLE (and Subtitle): Hydraulic Ram Studies | 5. TYPE OF REPORT & PERIOD COVERED: Master's Thesis, December 1973 |
| | 6. PERFORMING ORG. REPORT NUMBER |
| 7. AUTHOR(s): Wesley Richard Soper | 8. CONTRACT OR GRANT NUMBER(s) |
| 9. PERFORMING ORGANIZATION NAME AND ADDRESS: Naval Postgraduate School, Monterey, California 93940 | 10. PROGRAM ELEMENT, PROJECT, TASK AREA & WORK UNIT NUMBERS |
| 11. CONTROLLING OFFICE NAME AND ADDRESS: Naval Postgraduate School, Monterey, California 93940 | 12. REPORT DATE: December 1973 |
| | 13. NUMBER OF PAGES: 50 |
| 14. MONITORING AGENCY NAME & ADDRESS (if different from Controlling Office): Naval Postgraduate School, Monterey, California 93940 | 15. SECURITY CLASS. (of this report): Unclassified |
| | 15a. DECLASSIFICATION/DOWNGRADING SCHEDULE |

16. DISTRIBUTION STATEMENT (of this Report)

Approved for public release; distribution unlimited.

17. DISTRIBUTION STATEMENT (of the abstract entered in Block 20, if different from Report)

18. SUPPLEMENTARY NOTES

19. KEY WORDS (Continue on reverse side if necessary and identify by block number)

Hydraulic Ram
Ballistic Limit
Fiber Optics

20. ABSTRACT (Continue on reverse side if necessary and identify by block number)

Hydraulic ram concerns catastrophic failure of liquid filled tanks impacted by high speed projectiles. It is divided into four phases: entry/shock, pressure field, cavity, and free surface. The entry wall phase was investigated in detail.

A formula to predict energy losses of a bullet penetrating an aluminum plate is presented, and experimental data were obtained and compared.

A fiber optic transducer was designed to measure generated pressures in the shock and cavity phases.



EDITION OF 1 NOV 65 IS OBSOLETE
S/N 0102-014-6601

SECURITY CLASSIFICATION OF THIS PAGE (When Data Entered)

DD Form 1473 (BACK)
1 Jan 73
S/N 0102-014-6601

# Hydraulic Ram Studies

by

Wesley Richard Soper
Lieutenant, United States Navy
B.S., United States Naval Academy, 1967

Submitted in partial fulfillment of the
requirements for the degree of

MASTER OF SCIENCE IN AERONAUTICAL ENGINEERING

from the

NAVAL POSTGRADUATE SCHOOL
December 1973

Author Wesley Richard Soper

Approved by: Howard L Power
Thesis Advisor

J W Burden
Second Reader

Lickel
Chairman, Department of Aeronautics

Academic Dean

## ABSTRACT

Hydraulic ram concerns catastrophic failure of liquid filled tanks impacted by high speed projectiles. It is divided into four phases: entry/shock, pressure field, cavity, and free surface. The entry wall phase was investigated in detail.

A formula to predict energy losses of a bullet penetrating an aluminum plate is presented, and experimental data were obatined and compared.

A fiber optic transducer was designed to measure generated pressures in the shock and cavity phases.

TABLE OF CONTENTS

## LIST OF FIGURES

## TABLE OF SYMBOLS AND ABBREVIATIONS

| | |
|---|---|
| A | cross sectional area of cylindrical projectile |
| A(x) | cross sectional area of any projectile at given distance x |
| $E_i$ | kinetic energy at impact |
| $E_o$ | kinetic energy at ballistic limit |
| F | force |
| G | shear modulus of target material |
| m | mass of projectile |
| mil | .001 inches |
| P | penetration depth |
| R | distance from impact point to pressure probe |
| t | thickness of target |
| T | time |
| $V_e$ | exit velocity |
| $V_i$ | impact velocity |
| $V_o$ | ballistic limit |
| W | work |
| x | distance from nose of projectile to front wall of target |
| $\sigma_{y_T}$ | dynamic yield strength of target material |
| $\mu$ | micro = $10^{-6}$ in $\mu$seconds |
| m | milli = $10^{-3}$ in mseconds |

# I. INTRODUCTION

Since the days aircraft first began to fly in a hostile environment, the achievement of non-nuclear aircraft survivability has been the subject of extensive research. The ability of today's expensive air-to-air and air-to-ground weapons delivery systems to withstand hits by small arms fire and by warhead fragments is of paramount importance in this era of decreasing defense budgets.

An aircraft component which is easily hit and most susceptible to damage is the fuel tank. A damaged fuel cell can lead to aircraft loss in several ways, some of which are fire, explosion, fuel starvation, or fuel cell failure.

Catastrophic failure of a fuel tank due to impact by a high speed projectile is known as hydraulic ram. This is actually a misnomer, since the failure mechanism consists of four distinct phases rather than one quasi-static compression type of state. [Ref. 1]

The first phase, the entry/shock phase, is caused by the projectile compressing the fluid near the entry point to extremely high pressures. These pressures can range in the hundreds of thousands of pounds per square inch and cause a shock wave to move radially outward from the point of entry. However, the shock attenuates rapidly and, in general, is too weak to cause damage to the side and rear walls of the fuel tank; but it can cause outward bending of the wall in

the vicinity of the entry point and start cracks which can lead to eventual destruction of this wall.

At any given point in the tank a (relatively) slow pressure pulse begins when the attenuated shock wave reaches that point and continues with the passage of the projectile through the liquid. This phase is called the pressure field phase. Its pressures range in the hundreds of pounds per square inch and last for several milliseconds.

The third phase of hydraulic ram is called the cavity phase. As the projectile moves through the fluid it must displace the fluid from its path. A large radial velocity is thus imparted to the fluid, and, as a result, the fluid moves away from the projectile path creating a cavity. Existing fluid pressures (gravity and pressures caused by tank boundaries) eventually halt cavity growth and cause the onset of collapse. Inside the cavity are fluid vapors and trapped air which entered during wall penetration. As the cavity collapses this air is compressed to a high pressure resulting in re-expansion of the cavity. Expansion and collapse repeat several times before all the stored energy is dissipated. Pressures during this phase are of the order of one thousand pounds per square inch.

These three phases combine to impart a large velocity to the upper free surface of the liquid, if ullage is present, which in turn imparts an impulsive load on the top of the tank. This fourth phase of hydraulic ram is known as the free-surface phase.

The structural response to hydraulic ram is brought about by the transfer of energy (projectile to fluid, fluid to walls, etc.). The failure mode is a function of how this energy is distributed among the four phases. In this study the projectile energy loss during entry wall penetration was investigated in detail and compared with experimental results. There are two areas of bullet penetration studies: those assuming a plate of finite thickness which the projectile passes through and those concerning a plate of thickness greater than the penetration depth. The effect of projectile shape on penetration distance and energy loss by a projectile passing through a finite thickness plate were considered in this study. In order to be able to predict energy transferred to the fluid by the projectile during the shock phase and later during the cavity phase, a knowledge of energy losses during entry wall penetration is essential.

Knowledge of pressures during the three final phases of hydraulic ram is important because the major damage occurs during them. Fiber optic pressure transducers were designed in order to experimentally measure these pressures. The magnitude and duration of pressures during the shock and cavity phases were examined, and transducers were designed which are capable of accurately measuring these characteristics.

## II. ANALYTICAL PENETRATION STUDIES

In order to predict the phenomena taking place as a projectile impacts and passes through a plate, an analytical study of the entry wall phase of hydraulic ram is presented.

An essential assumption of this study of projectile impact, and the assumption made by Dunn in Ref. 2, is that "there exists in each unconstrained material body at constant, uniform initial temperature a dynamic yield strength, $\sigma_y$, that is a constant of the material." Therefore there is one well-defined material constant which can be used to predict penetration data.

This dynamic yield strength, when multiplied by the area of the projectile, A(x), which resists the motion, gives an estimate of the force retarding the bullet. An additional assumption is that the dynamic yield strength of the projectile is much greater than that of the target so that no substantial deformation of the projectile occurs. For these assumptions the retarding force is given by

$$F = -\sigma_{y_T} A(x) \tag{1}$$

where $\sigma_{y_T}$ is the yield strength of the target. Thus the projectile equation of motion is

$$\ddot{x} + \frac{\sigma_{y_T}}{m} A(x) = 0 \tag{2}$$

where $\ddot{x}$ is the acceleration of the projectile mass m. One

salient feature of equation (2) is that the force retarding the projectile is only a function of x. It is assumed that there is no plastic deformation of the target material and no significant frictional force during penetration.

Equation (2) was used for two types of penetration solutions: those concerning impact into a plate of thickness greater than penetration depth, and those concerning the passage of projectiles through thin plates.

For the first case, multiplying (2) by $\dot{x}$ and integrating yielded

$$(\frac{15m}{G})^2 (\dot{x}^2 - V_i^2) = - \int_0^P A(x)\, dx \qquad (3)$$

where G is the shear modulus of the plate and approximately equal to $\sigma_{y_T}/15$ [Ref. 2], $V_i$ is the impact velocity, and P the penetration depth.

Equation (3) was solved numerically by a computer program. The program, for a given impact velocity, determined the bullet trajectory parameter V as a function of incremental values of x until zero velocity was reached at the penetration depth. Figure 1 shows penetration depth vs. impact velocity for forty-five grain projectiles of three shapes. As expected, projectiles with a smaller cross-sectional area gradient penetrated further for a given impact velocity.

The second penetration problem considered was that for a given plate thickness. Unlike the first case, where the

effective retarding force area distribution A(x) increased until it reached a constant maximum value, A(x) for a thin plate of given thickness increased only until the nose of the projectile penetrated the backside of the plate. At that time A(x) decreased due to projectile protrusion from the backside of the plate. Figure 2 shows two stages of projectile penetration. It should be noted that the x-coordinate moves with the projectile so that x is defined as the distance from the nose of the bullet to the front side of the plate. In Figure 2a the bullet has partially penetrated the plate. The effective retarding area is shown as $A_{eff}$. In Figure 2b the nose of the projectile has penetrated the back side of the plate and $A_{eff}$ is the annular area shown. Thus, as the maximum cross-sectional area reaches the backside of the plate, the area resisting motion goes to zero. It is at this point that penetration is complete. The minimum impact velocity which a projectile must possess to ensure its reaching this point is defined as the ballistic limit.

The work done on the projectile during its deceleration in the plate is equal to the change in kinetic energy during penetration. An integration of the total retarding force during penetration yeilds

$$W = \sigma_{y_T} A_{max} t \qquad (4)$$

where t is the thickness of the plate. It is seen that the volume swept out by the projectile determines the penetration

energy loss, and the energy loss is totally independent of projectile shape. Alternately stated, this result predicts that, for a projectile of given mass and $A_{max}$, the ballistic limit is independent of projectile shape.

With this in mind, equation (2) was solved assuming a constant cross-sectional area, that is, assuming a cylindrically shaped projectile. The equation of motion was integrated twice with appropriate initial conditions substituted to yield:

$$x = V_i T - \frac{GA}{15m} \frac{T^2}{2} \tag{5}$$

where T is time and A is the projectile cross-sectional area.

For a projectile with a velocity of $V_i$ impacting a plate of thickness t and exiting with a velocity of $V_e$, from (5) above,

$$t = V_i T - \frac{GA}{15m} \frac{T^2}{2} \tag{6}$$

and

$$V_e = V_i - \frac{GA}{15m} T \tag{7}$$

Solving (7) for T and substituting into (6) and solving for $V_e$ yields

$$V_e = [\, V_i^2 - \frac{GA}{15m} t \,]^{1/2} \tag{8}$$

At the ballistic limit, the exit velocity is zero, hence equation (8) was solved for $V_i$ (denoted as $V_o$ to designate

ballistic limit):

$$V_o = \left[ \frac{GA}{15m} t \right]^{1/2} \qquad (9)$$

A relationship between the impact velocity, the exit velocity, and the ballistic limit can be found by substituting (9) into (8) and solving for $V_e$:

$$V_e = V_o \left[ \left(\frac{V_i}{V_o}\right)^2 - 1 \right]^{1/2} \qquad (10)$$

Equation (10) shows, for impact velocities much higher than the ballistic limit, that the exit velocity approaches the impact velocity.

Equation (10) may also be used to find an estimate of the percentage of energy loss for a projectile which penetrates a finite thickness plate:

$$\%E_{lost} = \left[ \frac{E_o}{E_i} \right] 100 = \left[ \frac{GA}{15m} t \right] \left[ \frac{1}{V_i^2} \right] 100 \qquad (11)$$

where $E_o$ is the projectile kinetic energy when traveling at the ballistic limit, and $E_i$ is the energy at impact velocity.

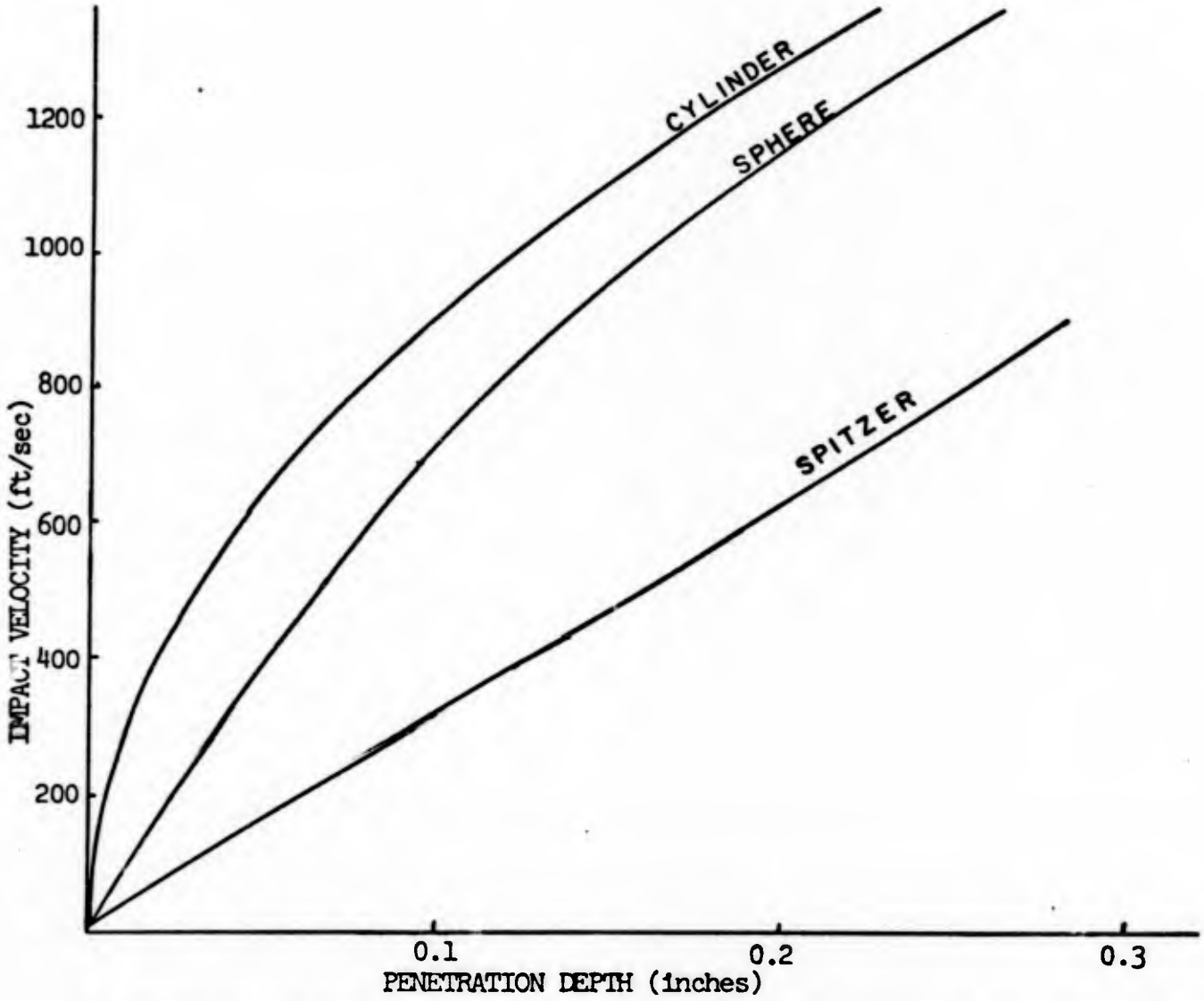


FIGURE 1. Penetration Depth vs. Impact Velocity for a Semi-Infinite Aluminum Target

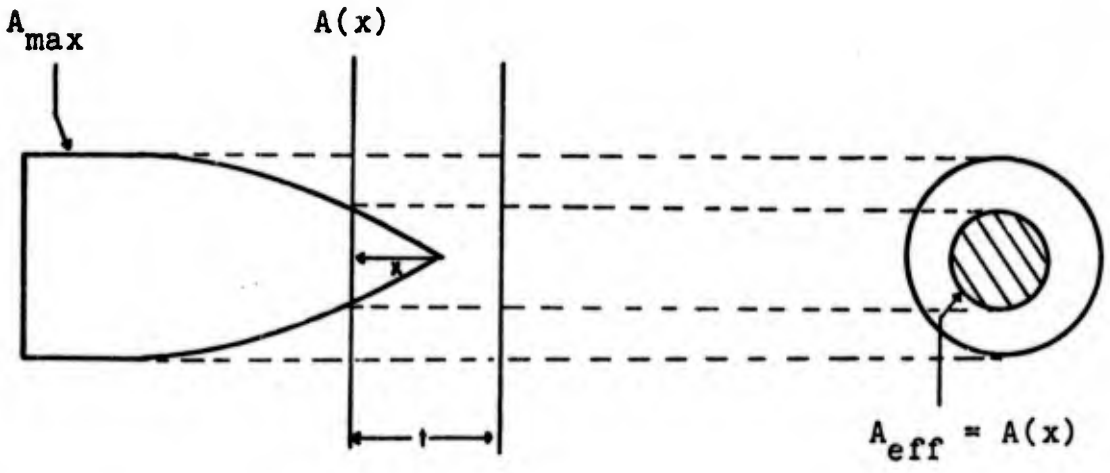


a. Early Stage

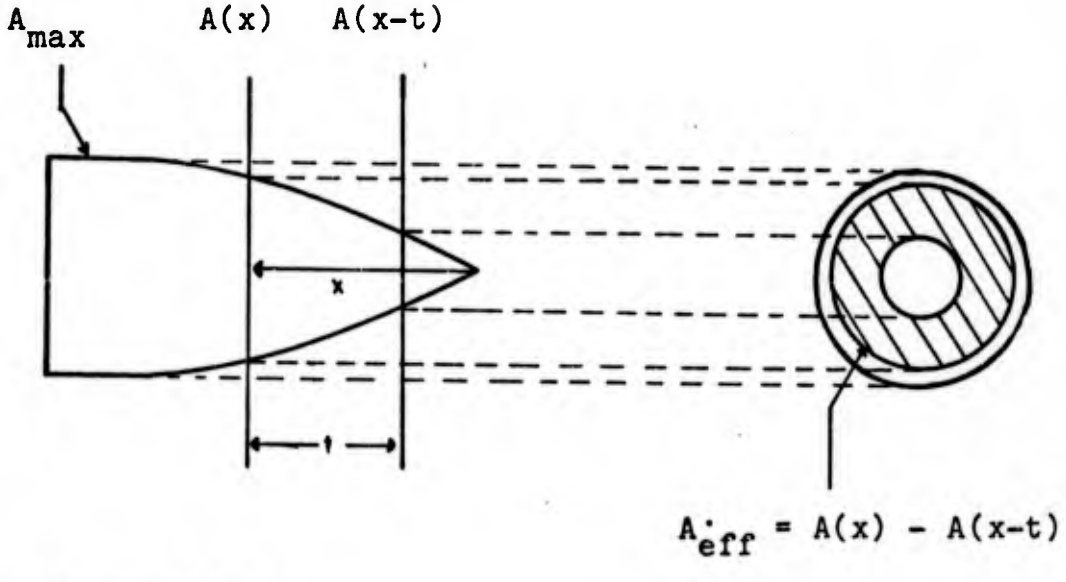


b. Protrusion Stage

FIGURE 2. Stages of Projectile Penetration

## III. EXPERIMENTAL STUDY OF ENTRY WALL PENETRATION

Figure 3 shows the basic components of the ballistic range used in the experiments. They were the rifle and its mount, chronograph screens and counters, aluminum test plate and holder, shadowgraph station, and bullet catcher.

The rifle mounting system, shown in Figure 4, consisted of the rifle mount and an adjustable rigid rifle mount stand. The system was designed to hold rifles of .22, .222, and .30 caliber. In this study, a .222 Remington was used. The bullets utilized were of a mass of forty-five grains and of two shapes, hornet and spitzer. Projectile impact velocities ranged from 2400 to 3000 feet per second.

The velocity was measured by three chronograph screens, AVTRON No. A914T333, mounted six feet apart. Each screen had a five-volt D.C. signal across it. When the screen was broken by a bullet, a pulse was sent to a counter. The first sensor started the first counter. The second sensor simultaneously stopped the first counter and started the second. The third sensor stopped the second counter. Thus the average velocity between counters was obtained, allowing a prediction of the impact velocity at the plate. A typical chronograph station is shown in Figure 5. Also shown in this figure is a shadowgraph apparatus which was not utilized during this phase of testing. The counters used were Monsanto 101B 1MHz. The trigger error was less than $\pm$ 0.3% of one period for sine waves with signal-to-noise ratio of 40 db or better.

The empty fuel tank entry wall was simulated by a three-inch by four-inch 7075-T6 aluminum plate. Three thicknesses, 0.05 inches, 0.09 inches, and 0.16 inches were tested. Early in the test phase it was determined experimentally that the size and method of supporting the test plate had no significant effect on the exit velocity of the projectile.

In addition to stopping the second counter, sensor three was used to trigger the delay unit which generated a pulse which could be time delayed from 190 μseconds to 1700 μseconds. The delay unit circuitry is shown in Figure 6. The delayed pulse was then used to trigger a spark source just after bullet penetration of the plate. The light from the spark source was directed to a film plate by a concave mirror on the opposite wall. The mirror collimated the light which then passed behind the test plate and onto the film. In this manner, shadowgraphs were taken to examine the shape of the bullet after it had passed through the plate. The shadowgraphs also showed the resulting flow field behind the plate. Figure 7 shows the spark source and mirror as they were set up.

The chronograph screens mounted directly behind the test plate were used to measure the velocity of the bullet as it exited the plate. Figure 8 is a photograph of this apparatus.

The bullet catcher is shown in Figure 9. The sides, top, and bottom were 1/2-inch aluminum. The three-foot square front had three 3/8-inch plywood baffles inserted into it. The back of the catcher was made of two plates of 3/8-inch

steel mounted at an angle of 45 degrees to the path of the bullet. This ensured bullet deflection downward into a layer of sand, reducing the likelihood of ricochets.

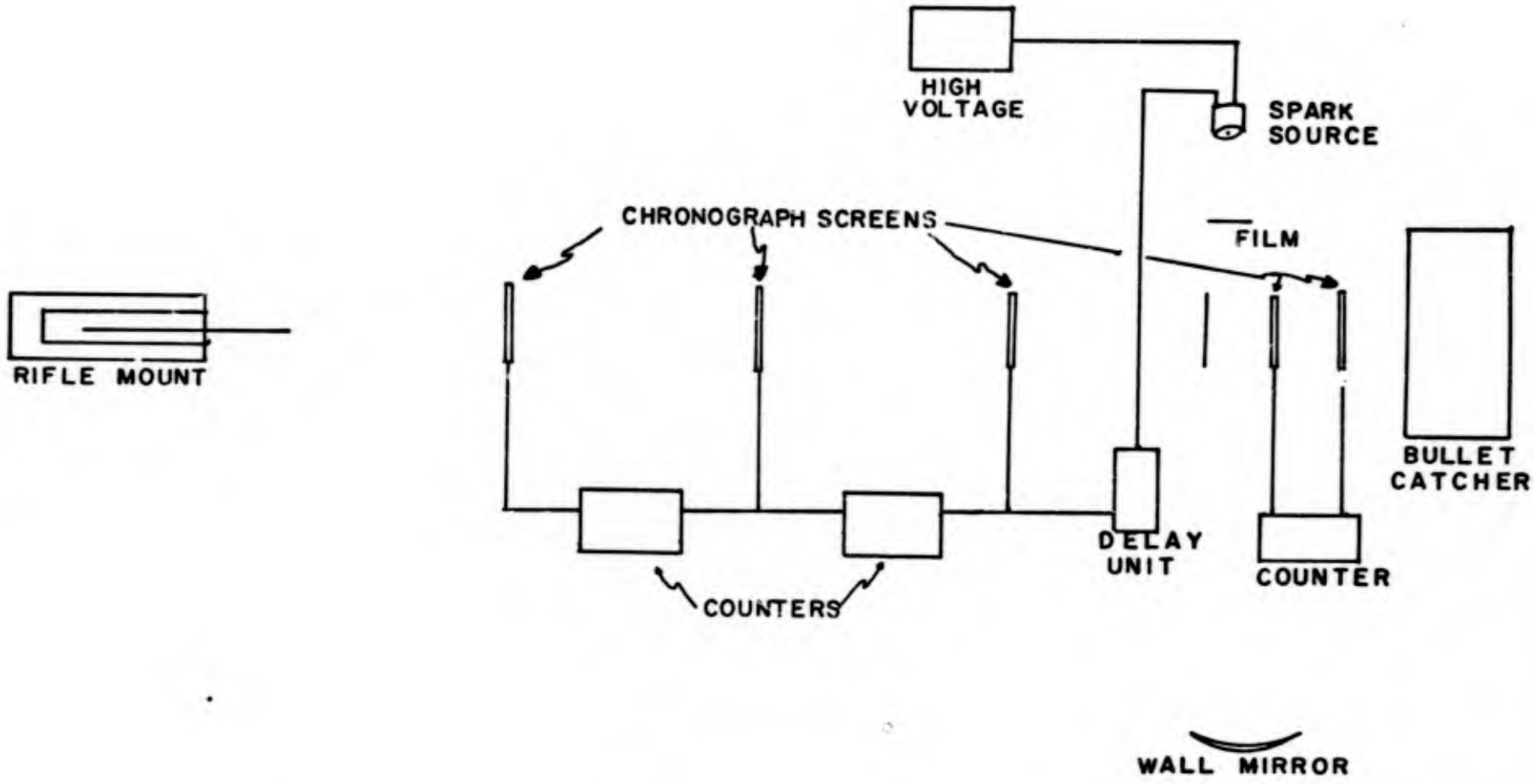


FIGURE 3. Ballistic range components.

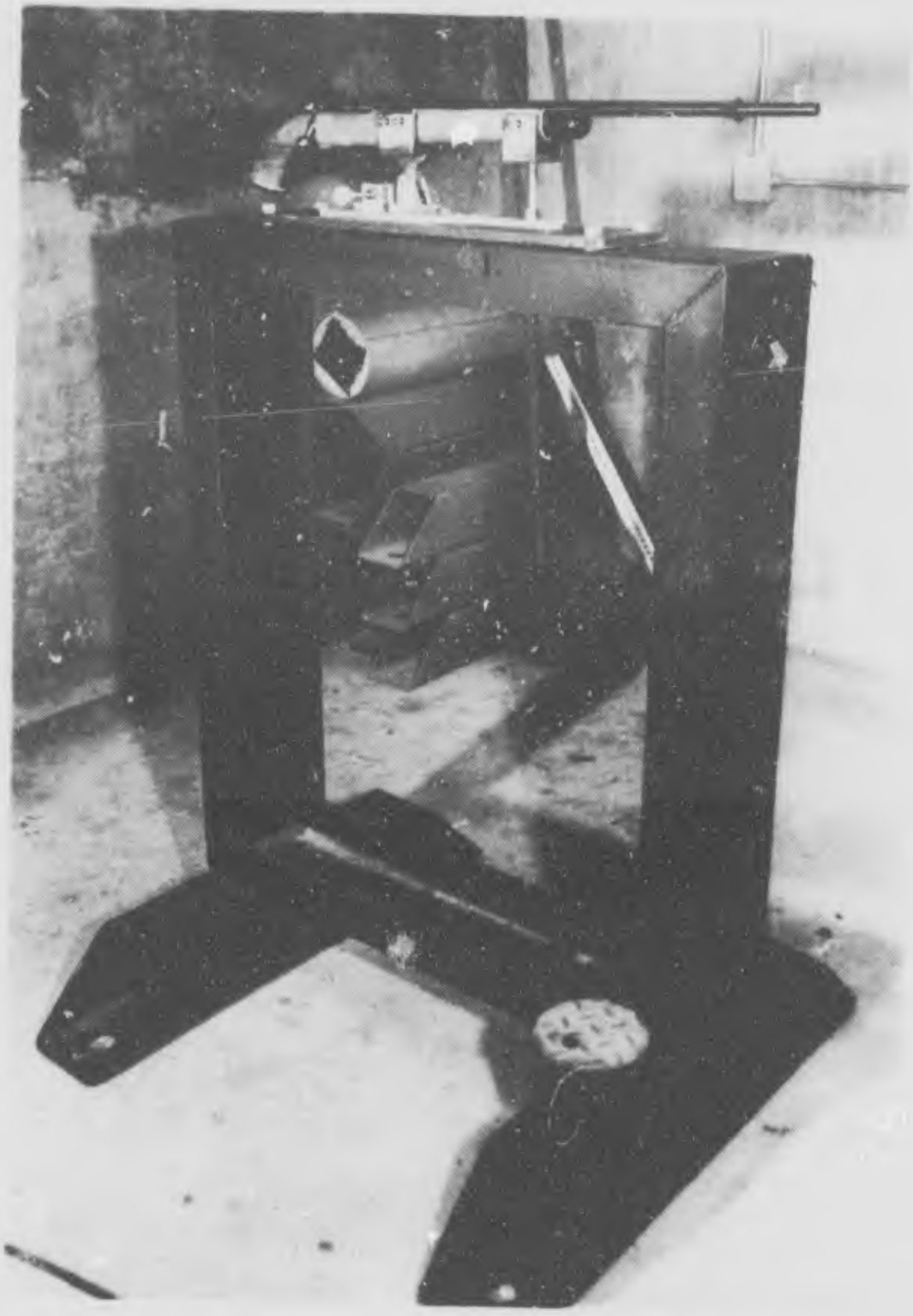

FIGURE 4. Ballistic Range Rifle Mounting System

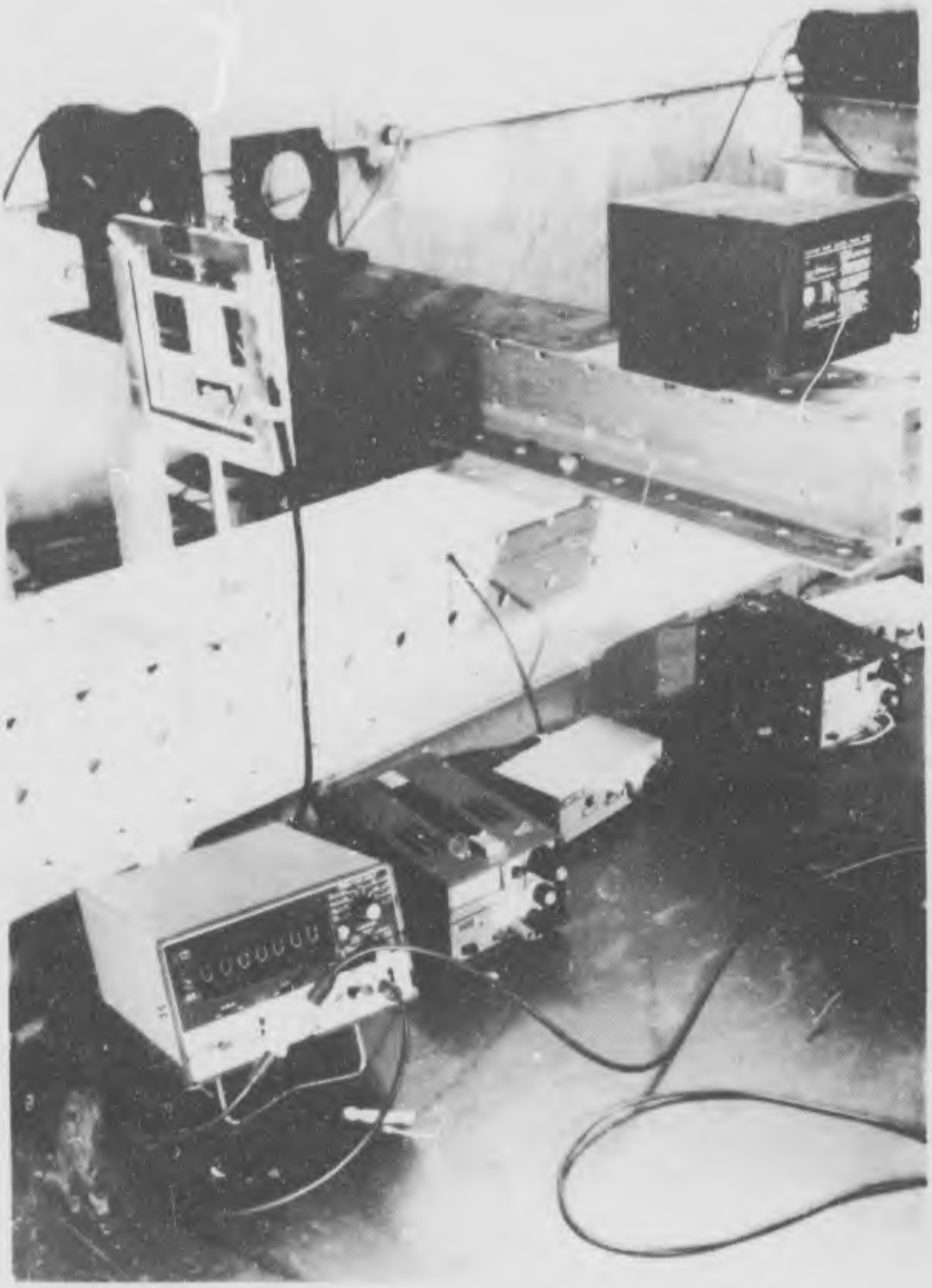

FIGURE 5. Ballistic Range Chronograph Station

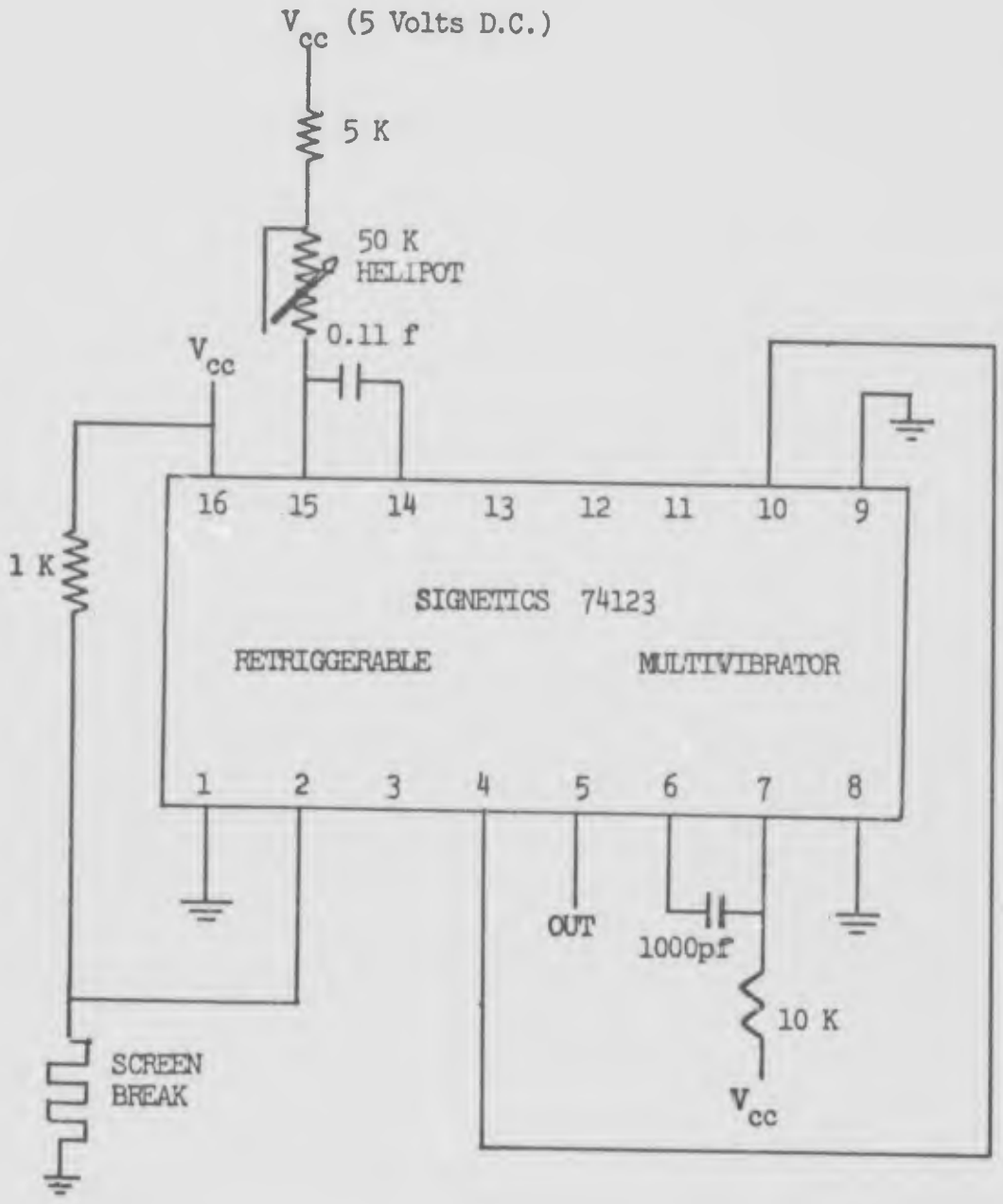


FIGURE 6. Delayed Pulse Generator Circuitry (Variable)

FIGURE 7. Spark Source and Mirror

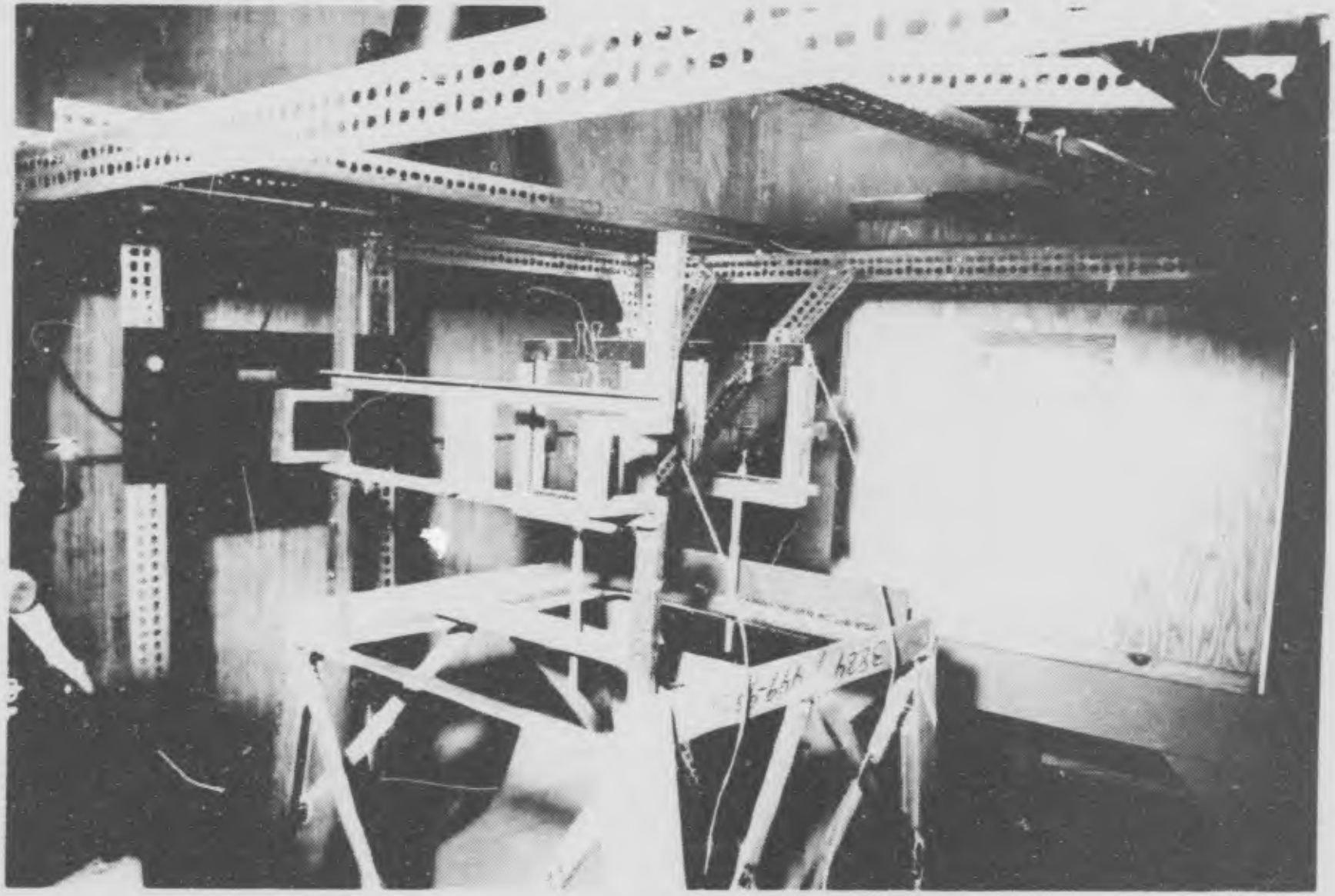

FIGURE 8. Test Plate and Chronograph Screens

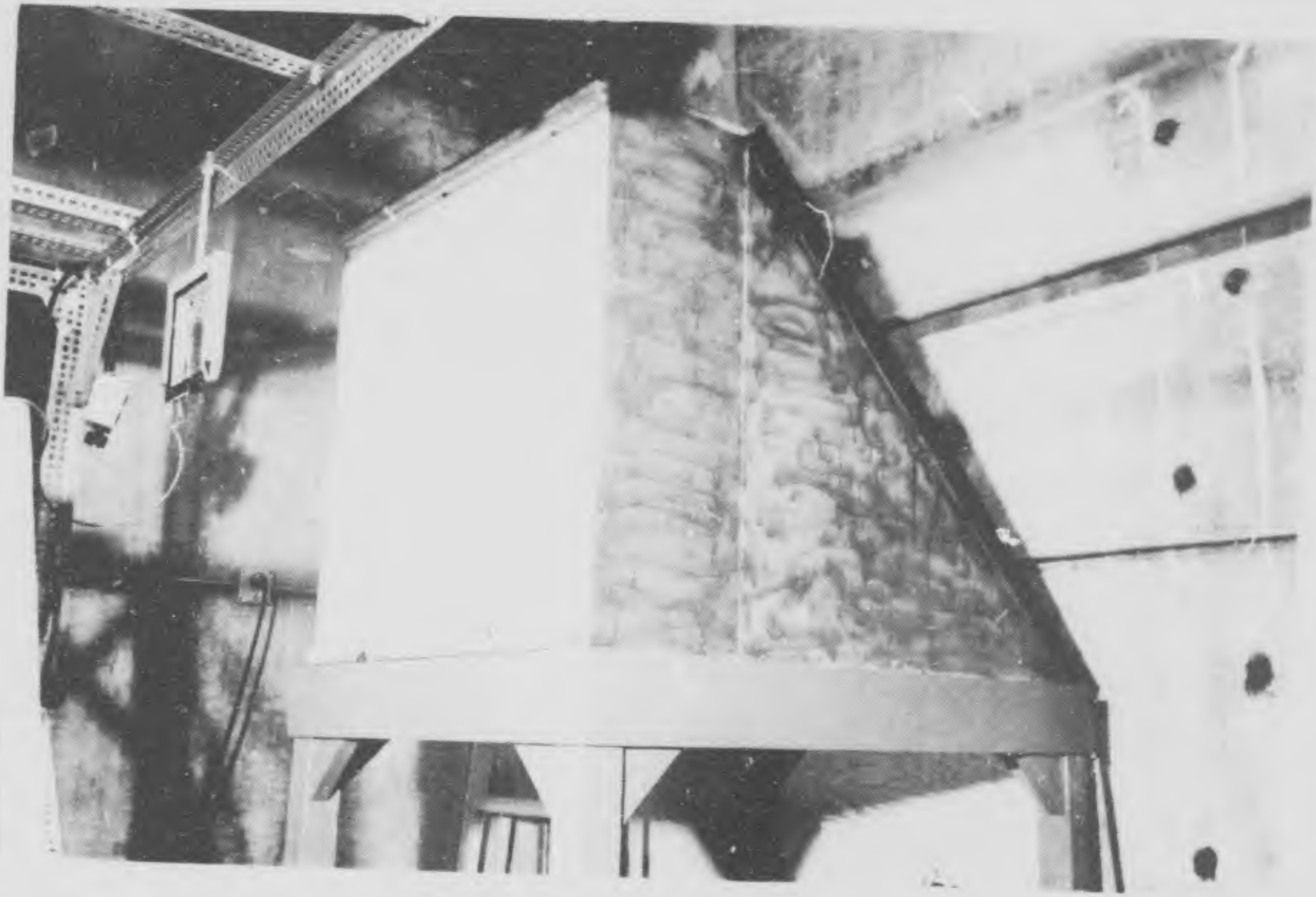

FIGURE 9. Ballistic Range Bullet Catcher

## IV. FIBER OPTIC PRESSURE TRANSDUCER DESIGN

### A. INTRODUCTION

An accurate means of measuring pressures generated during all phases of hydraulic ram is needed to assess the validity of any analytical studies. The most popular types of pressure measuring devices in use today are the semiconductor strain gauge and the piezoelectric transducer. Both costly and fragile, these devices are also sensitive to temperature changes and contamination from small dust particles. A fiber optic pressure transducer was designed in order to overcome these problems. Two optical glass fiber bundles were used, one to transmit light to the inner surface of the transducer diaphragm and one to collect and transmit reflected light to a photomultiplier tube. This signal output was then amplified and could be measured from a photograph of the resulting oscilloscope trace. The intensity of the output light, being a function of displacement between the fiber bundle and the diaphragm, was thus made a measure of pressure on the diaphragm. A possible arrangement of the pressure measuring apparatus is shown in Figure 10.

The fiber optic transducer is in reality a proximity gauge. Because pressure on the diaphragm causes it to deform slightly and decrease the distance between the diaphragm surface and the fiber ends, output can be read in terms of pressure increase rather than distance decrease.

Figure 11a, obtained from Ref. 6, shows two fibers, one emitting light and one collecting light. As the displacement between the fiber ends and the diaphragm increases, the cone of light from the transmitting element illuminates an increasingly larger area of the diaphragm. The light reflected from the diaphragm becomes a cone of light, increasingly intense as the diaphragm moves away from the fiber ends. Figure 11b shows typical output of the receiving fibers vs. fiber-diaphragm displacement. The front side of the curve indicates linearity between output and distance. As the distance increases, however, the cone of light from the transmitting fiber fills the entire diaphragm, and the curve reaches its peak. Beyond this point, the intensity of light to the receiving element decreases as the inverse of the distance squared [Ref. 6].

## B. DESIGN CONSIDERATIONS

Due to the great disparities between the peak pressures and the time scales of the pressure signals in the shock and cavity phases of hydraulic ram, two separate pressure transducer designs are necessary. Figure 12 shows the basic geometry of both transducers. In addition to the optical fiber probe, the transducers consist of an outside tube and a diaphragm silver soldered or welded to the tube end. A sleeve is required inside the tubing to ensure orthogonal orientation of the probe tip to the diaphragm.

Linear response of the pressure transducers is desired, and in order to achieve this the maximum deflection of the diaphragm is limited to less than half its thickness. This allows the light transmission to remain on the linear portion of the displacement curve of Figure 11. The resonant frequency of the diaphragm must be large enough to provide adequate frequency response to the transducer. Finally, the pressure transducer must be able to withstand the maximum pressures occurring during hydraulic ram and should be placed so that the diaphragm is flush with the tank wall when measuring shock phase pressures. The transducer should be isolated from wall vibration, if any; therefore, it was insulated by a seal made of RTV.

C. SHOCK PHASE DESIGN

Figure 13 shows peak pressures (predicted by the strong shock theory of [4]) encountered at various distances from point of impact of a .30 caliber projectile penetrating the fluid at 3000 fps and an energy of 34,000 ft-lb. Measurable pressures are of duration of about 12 μsec and a pressure transducer placed approximately 1.4 inches from the point of initial impact will experience a peak pressure of $7.8 \times 10^4$ psi, 12 μsec after impact. Figure 13a indicates that the shock pressure signature can be approximated by the sawtooth function shown in Figure 13b. The Fourier Expansion of the sawtooth is given by

$$f(x) = \frac{1}{4} + \sum_{k=1,3,5..}^{n} \left\{ \frac{-2}{\pi^2 k^2} \cos kx + \frac{(-1)^k}{\pi k} \sin kx \right\} \quad 0 \leq x \leq 2\pi \quad (12)$$

where $a_k = \frac{-2}{\pi^2 k^2}$ and $b_k = \frac{(-1)^k}{\pi k}$ .

For adequate frequency response of the transducer, it is desired that the amplitude of the high frequency signal content be at most ten percent of the fundamental amplitudes $a_k$ and $b_k$. For $a_k$ proportional to $k^{-2}$, the smallest value of k that meets this requirement is 5. However, $b_k$ is proportional to $k^{-1}$ and thus the smallest value of k is 11. The high frequency content of the shock pressure signal is then approximately k/24 μsec or 0.46 MHz.

Requiring the transducer to be capable of measuring peak pressure of 100,000 psi, Figure 15, obtained from Ref. 3, shows that the minimum diaphragm thickness is 23 mils. According to Figure 16, all stainless steel diaphragms of sufficient diameter (greater than 0.160 inch to accommodate the .109-inch fiber bundle) have resonant frequencies near the operating frequency. A diaphragm 35 mils thick and 0.160 inches in diameter has a resonant frequency of 0.5 MHz and has a maximum deflection of just under 1 mil at 100,000 psi. Because the fiber optic system output resolution is approximately 0.01 mils, only pressures above 1000 psi can be measured for this proposed design.

## D. CAVITY PHASE DESIGN

The geometry of a transducer measuring pressures during the cavity phase must be different from that required to measure pressures during the shock phase due to lower pressures acting over longer periods of time during cavity collapse.

Figure 14a, obtained from Ref. 5, indicates, for a 0.30 caliber projectile, maximum cavity collapse pressures were less than 1000 psi and each pulse lasted for approximately 0.5 msec. The pressures rose and fell at nearly the same rate, allowing the pressure signature to be approximated by a triangular wave, as shown in Figure 14b.

As in the previous analysis, the Fourier expansion of the triangular function yields:

$$f(x) = \frac{1}{2} - \frac{4}{\pi^2} \sum_{k=1,3,5\ldots}^{n} \frac{1}{k^2} \cos kx \qquad 0 \leq x \leq 2\pi \qquad (13)$$

Again the amplitude of the high frequency components must be 10% of the fundamental amplitude for adequate frequency response. The frequency response required by this pressure signal is then k/0.5 msec or .01 MHz.

A stainless steel diaphragm 10 mils thick with a diameter of 0.190 inches has a resonant frequency of very near 0.1 MHz, and is capable of withstanding peak pressures of 3000 psi. It is suggested that this geometry be used for the cavity phase transducer.

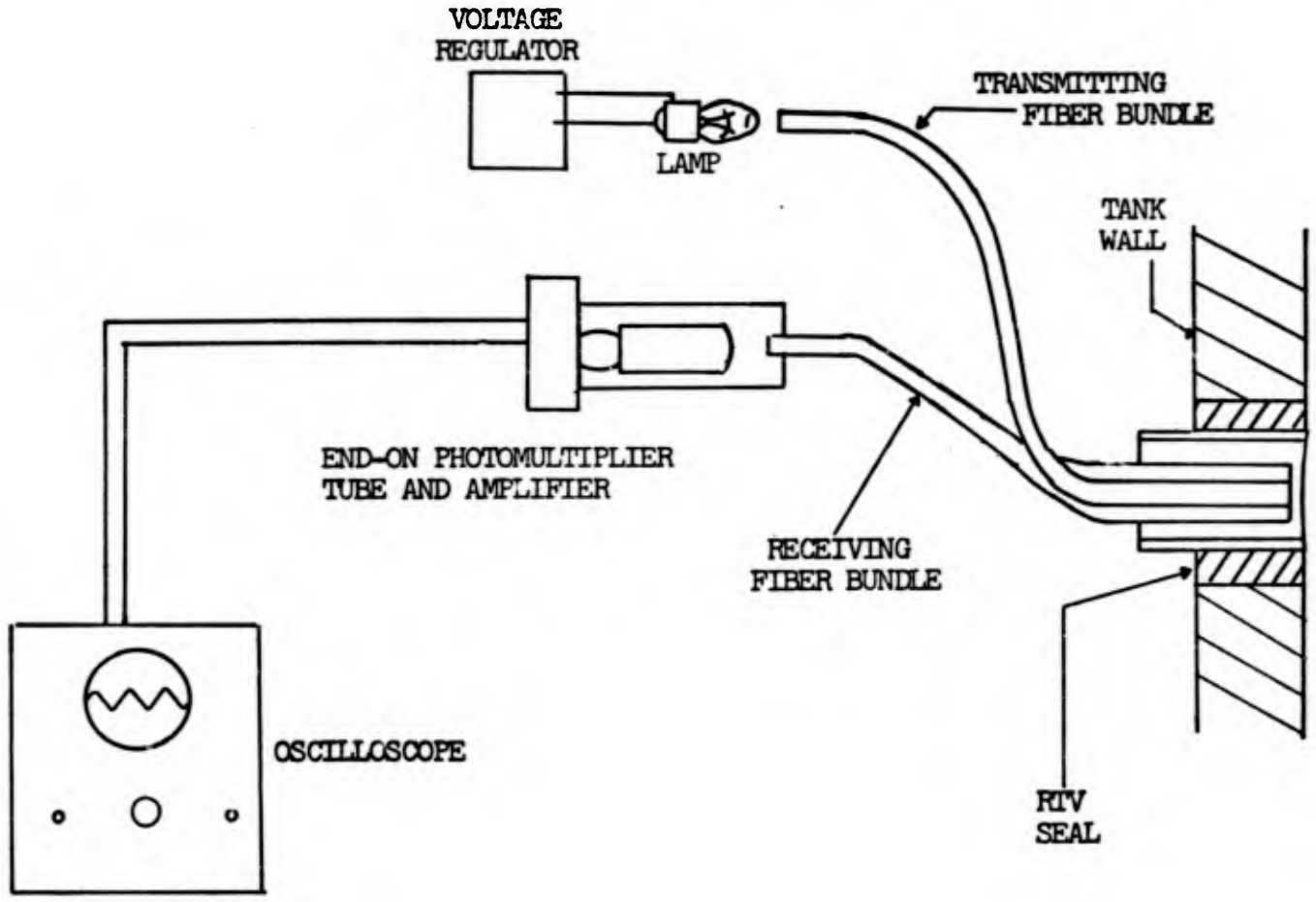


FIGURE 10. Experimental Arrangement of Fiber Optic Pressure Transducer

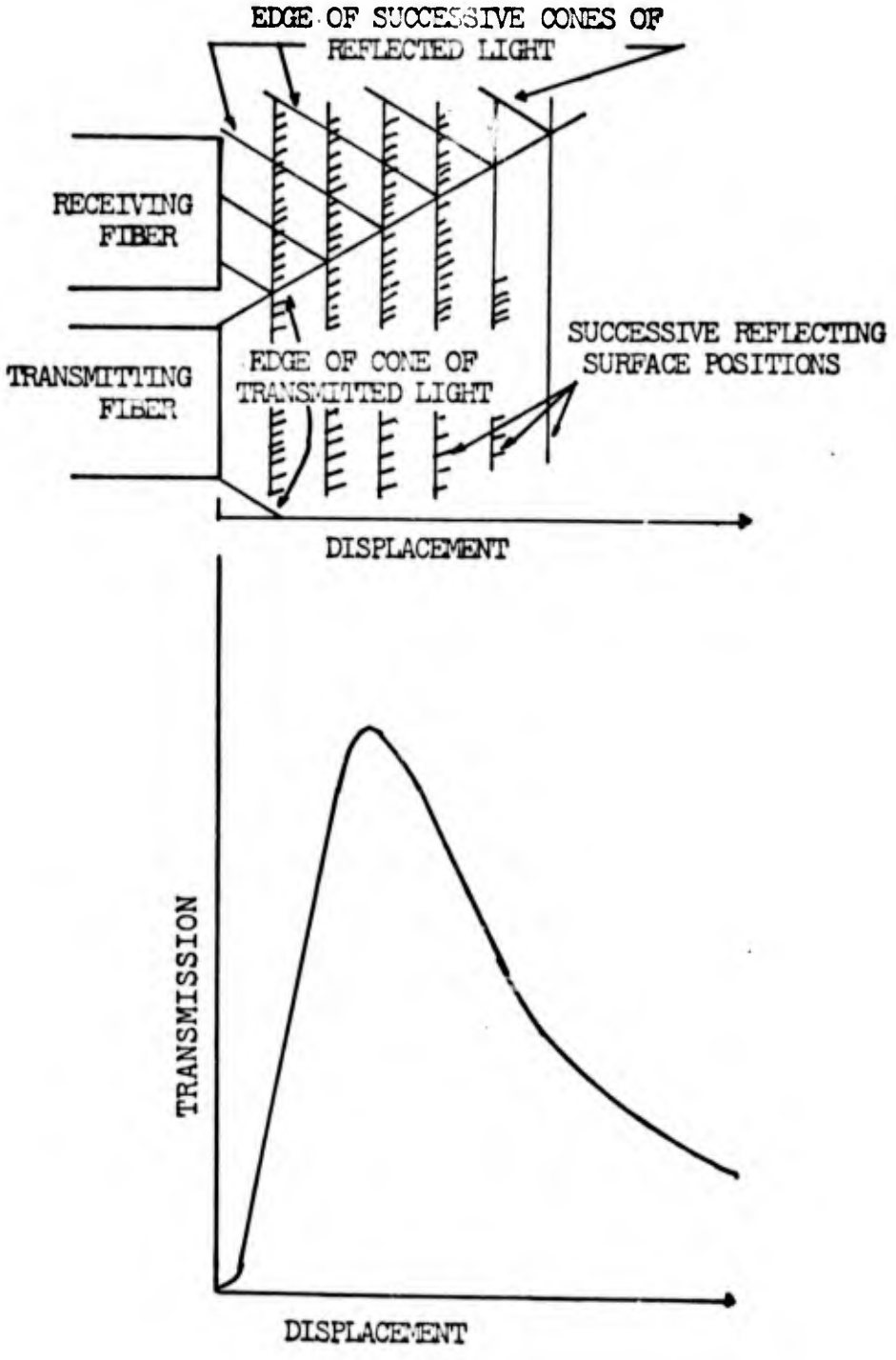


FIGURE 11. Displacement Measurement

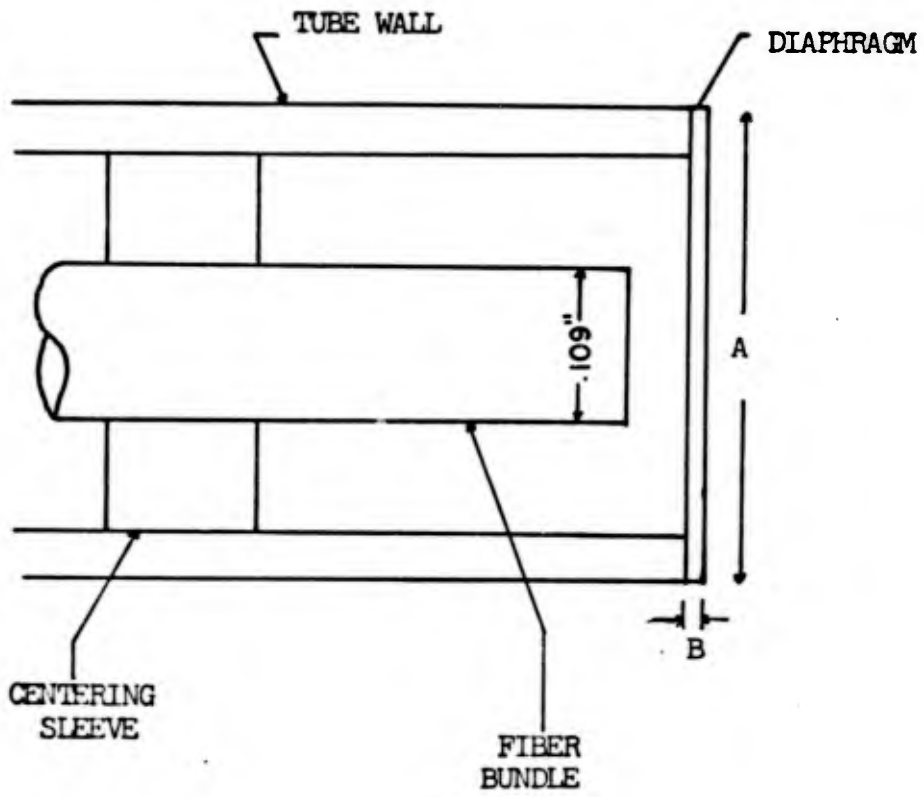


| PHASE | A | B |
|---|---|---|
| SHOCK | .160" | 35 mils |
| CAVITY | .190" | 10 mils |

FIGURE 12. Transducer Cross Section

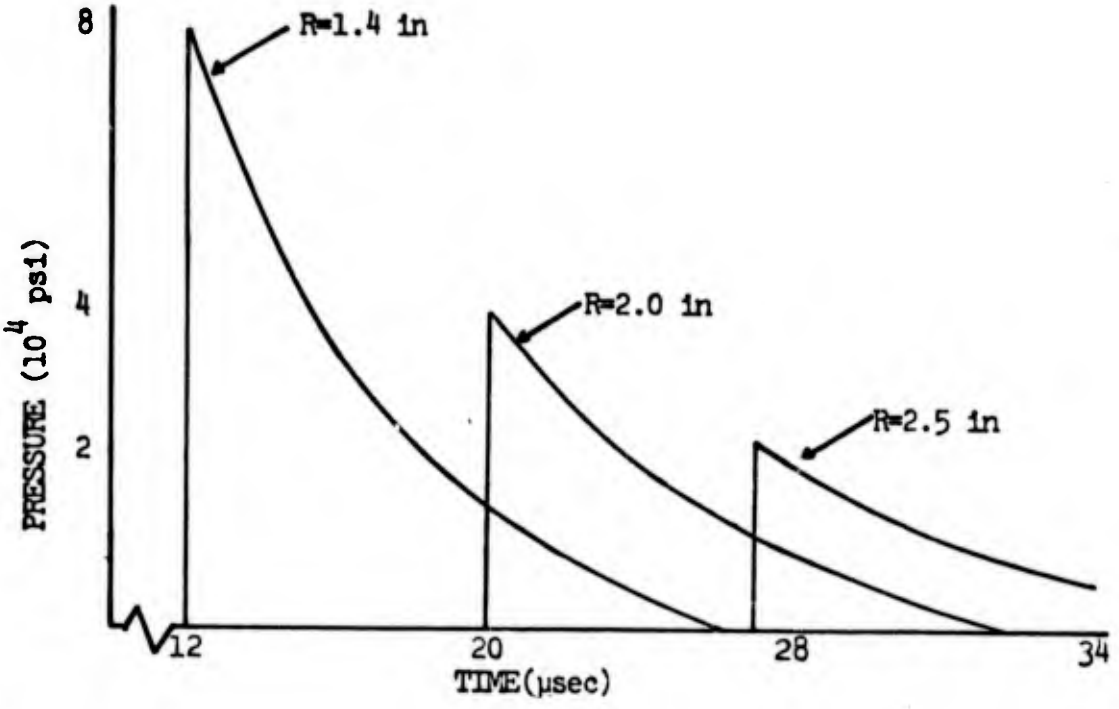


a.

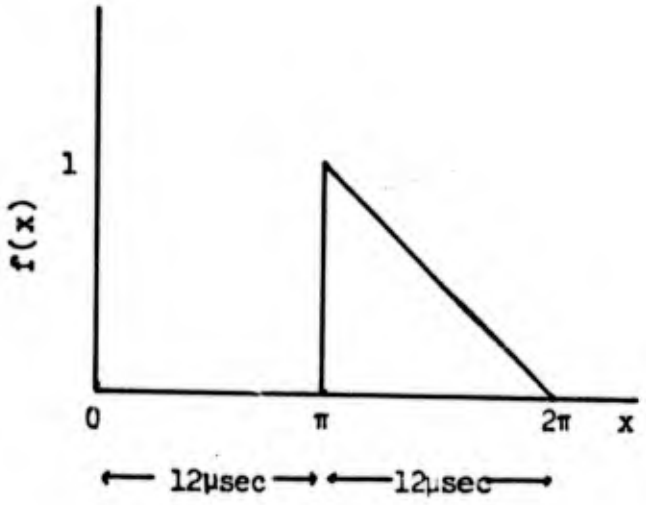


b.

FIGURE 13. Pressure Pulses and Sawtooth Representation for Shock Phase Pressure Signal

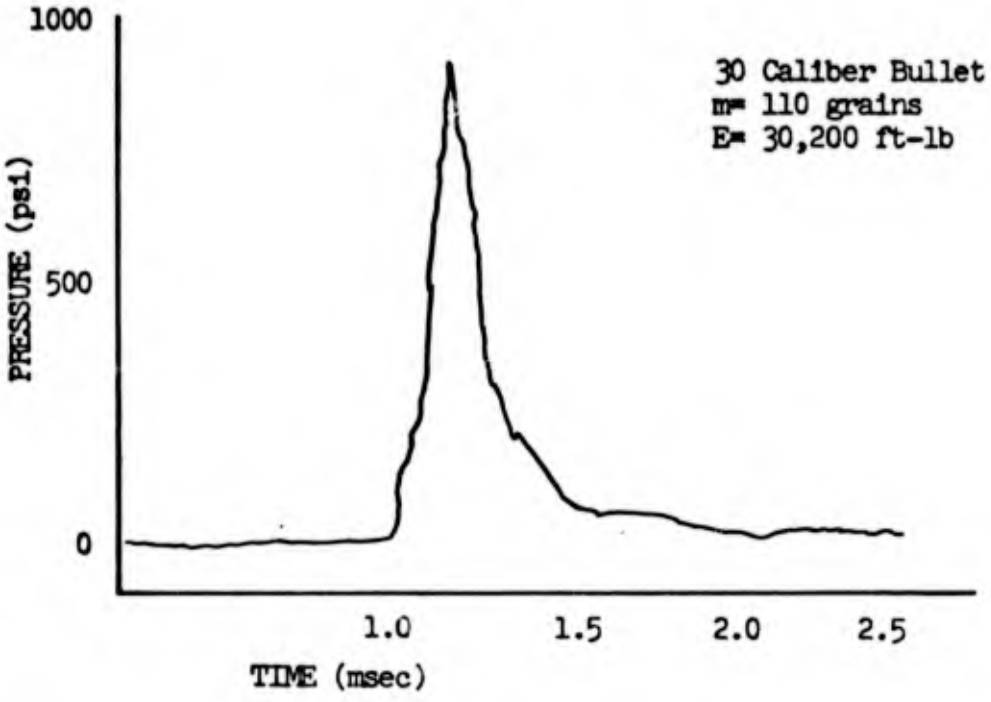


a.

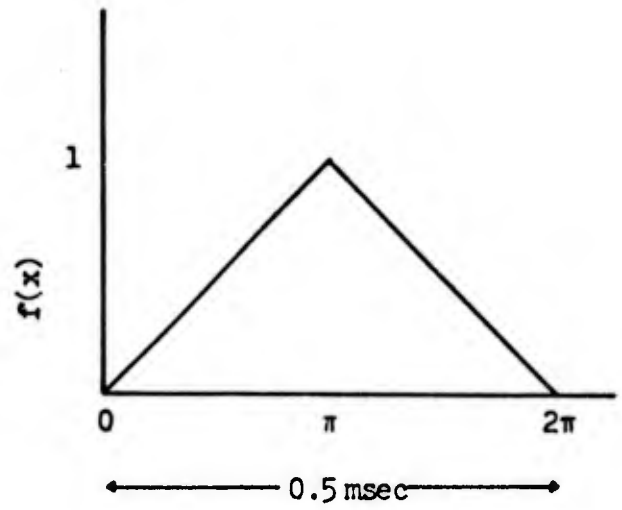


b.

FIGURE 14. Diaphragm Maximum Deflection

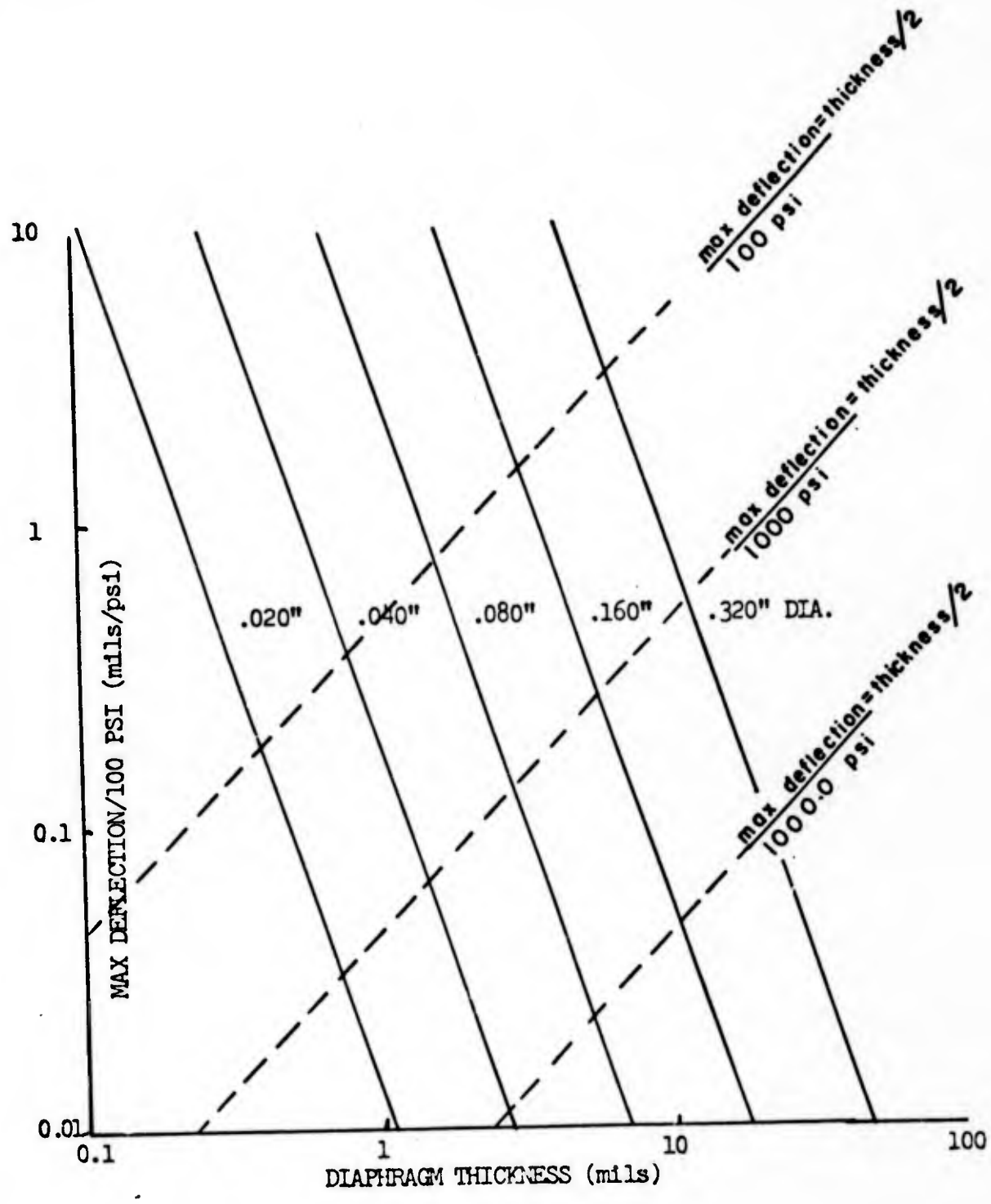


FIGURE 15. Diaphragm Maximum Deflection

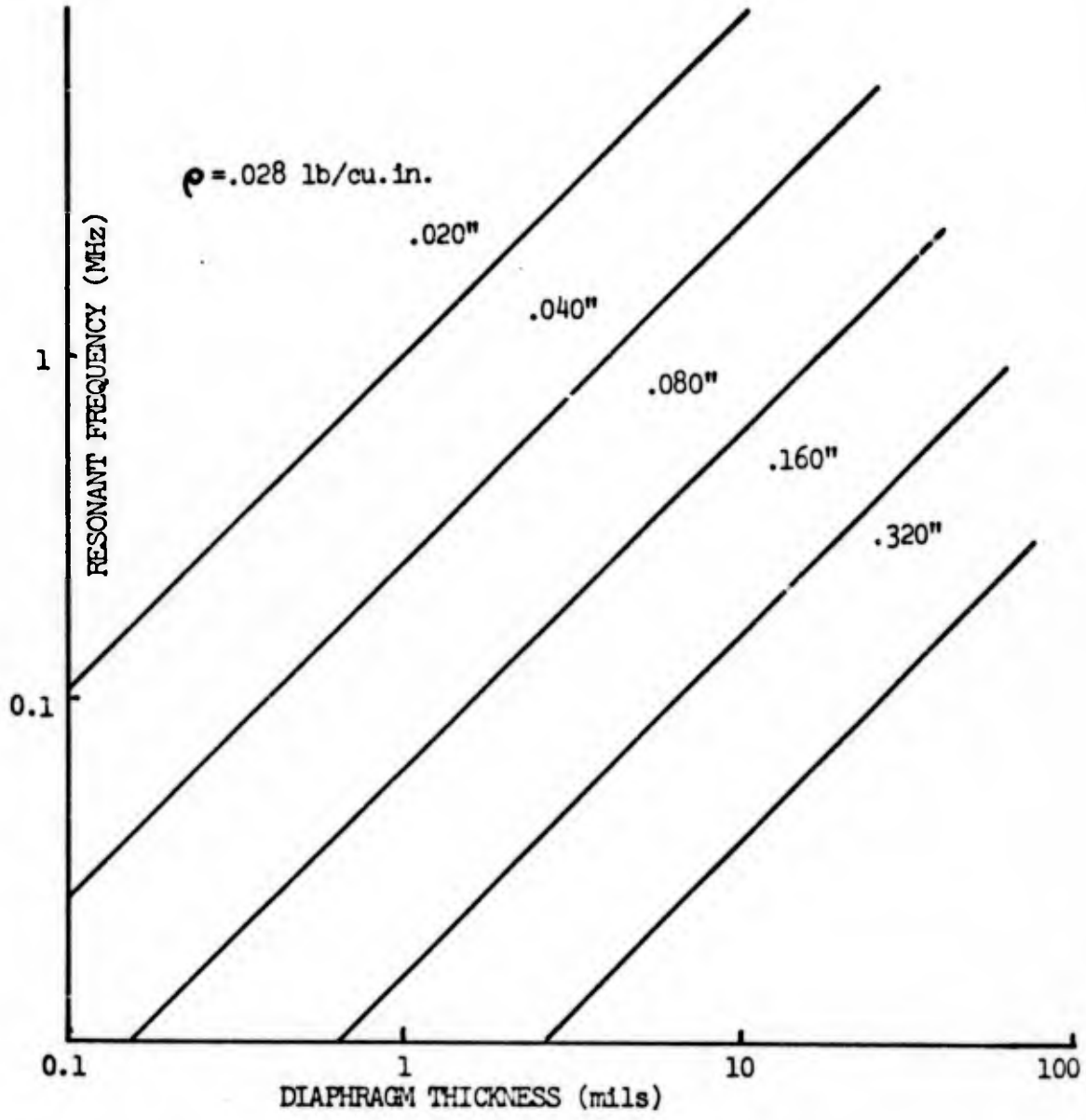


FIGURE 16. Diaphragm Fundamental Resonant Frequency

## V. RESULTS AND CONCLUSIONS

One important assumption made in the analytical study was that the yield strength of the projectile was significantly higher than that of the target material. However, the projectile was copper jacketed, and the yield strength of copper is approximately $0.39 \times 10^6$ psi as compared with $0.25 \times 10^6$ psi for aluminum. Figure 17 shows clearly that, although the projectile and target yield strengths are of the same order of magnitude, projectile shape was not altered during plate penetration, except very close to the nose of the projectile. Thus it can be concluded that for hypervelocity impact phenomena, the assumption only need be made that the yield strengths of the projectile and target materials be of the same order of magnitude.

The analytical result that projectile shape is not material in predicting penetration energy losses is also shown in the experimental results. Equation (9) was derived using that assumption. Figure 18 shows a plot of exit velocity vs. impact velocity for 45-grain projectiles of two shapes penetrating aluminum plates of three thicknesses. The solid lines are plots of Equation (10), using Equation (9) as the definition for ballistic limit. Because both shapes yielded similar data, no distinction between them was made. Data points agreed well with prediction leading to the conclusion that projectile shape does not, in fact, significantly affect energy loss through a plate.

The theoretical energy loss from Equation (11) was plotted vs. impact velocity in Figure 19. Experimental data again agree closely with prediction, reinforcing the concept that projectile shape has no significant effects on energy loss through thin plates.

It can be concluded, therefore, that a means is available whereby energy losses through a wall of an unfilled fuel tank can be predicted accurately and simply. This is the first step in finding energy transferred during the hydraulic ram phenomenon. Effects of fluid foundation on the penetration characteristics of the walls are expected to be minimal, but further experimental study of this effect should be undertaken.

It should be noted that all experimentation and analytical work in this study has been conducted using bodies of revolution that do not tumble. However, an application of the concept of the shape independence of energy loss can be made in the case of fragment penetration. This representation will only be applicable to early stages of hydraulic ram, as projectile shape does have major effects on the size and intensity of the cavity phase. Aircraft damage and penetration characteristics of fragments (such as from SAM warheads) may be approximated by cylindrical bodies of equal mass and maximum cross-sectional area. It is expected that fragment energy loss during wall penetration will follow Equation (11).

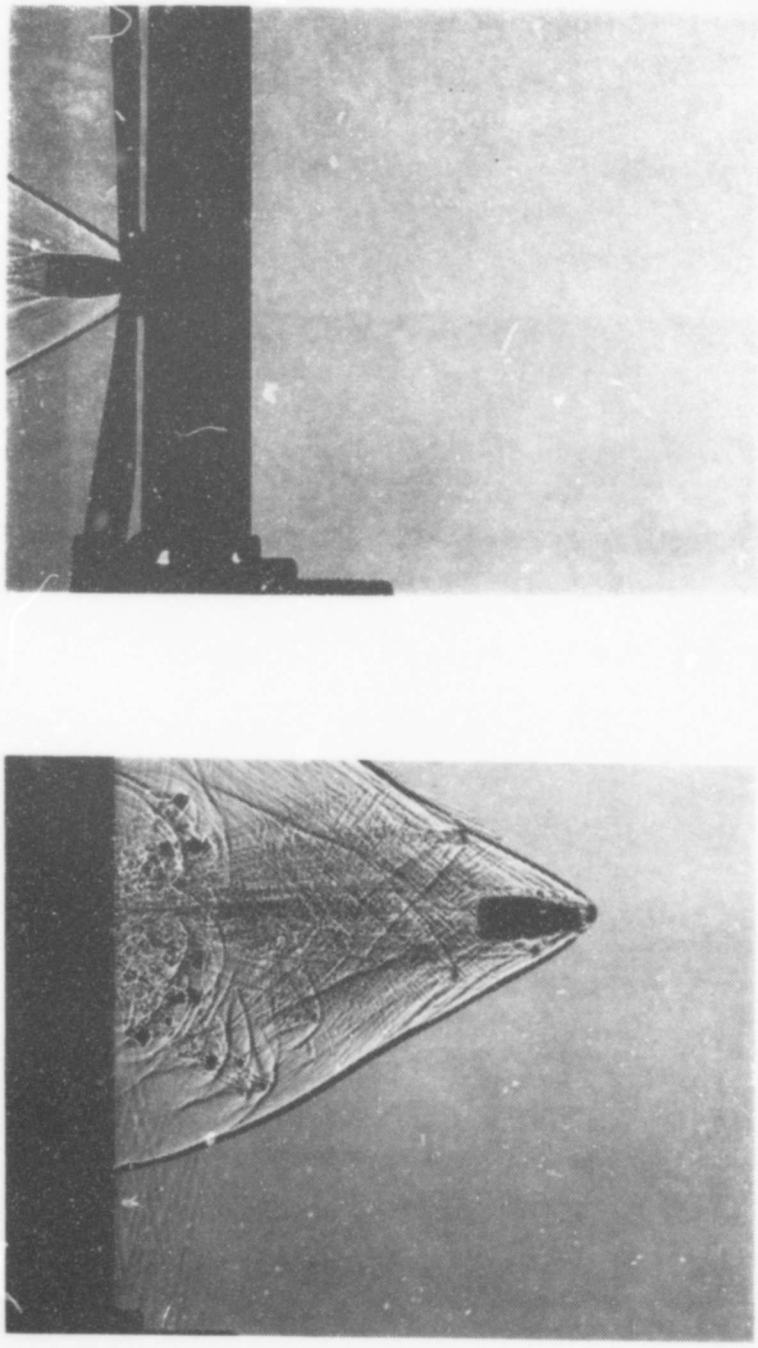

FIGURE 17. 45 Grain Spitzer Entering and Exiting Aluminum Plate

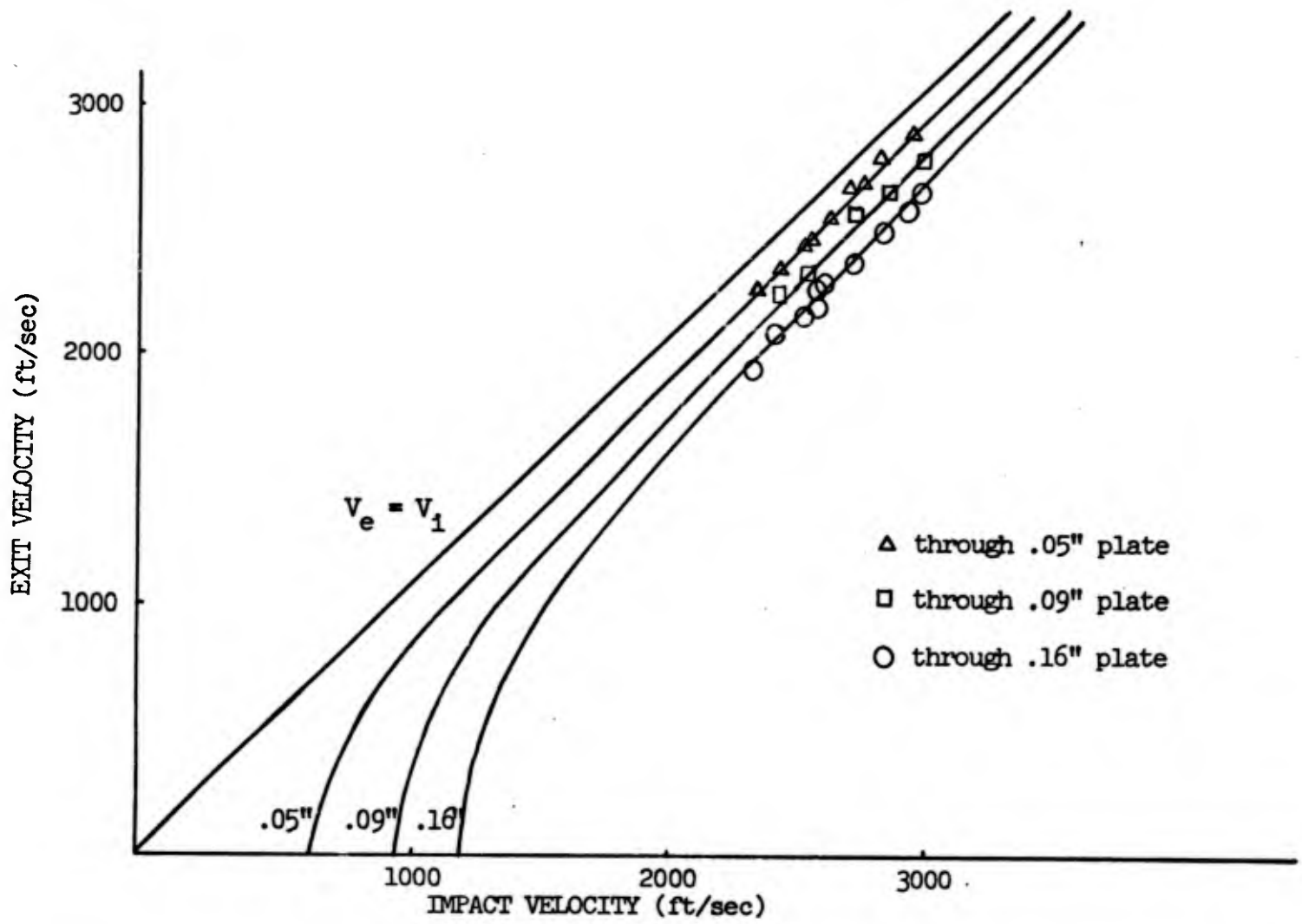


FIGURE 18. Impact Velocity vs. Exit Velocity for Plates of Three Thicknesses

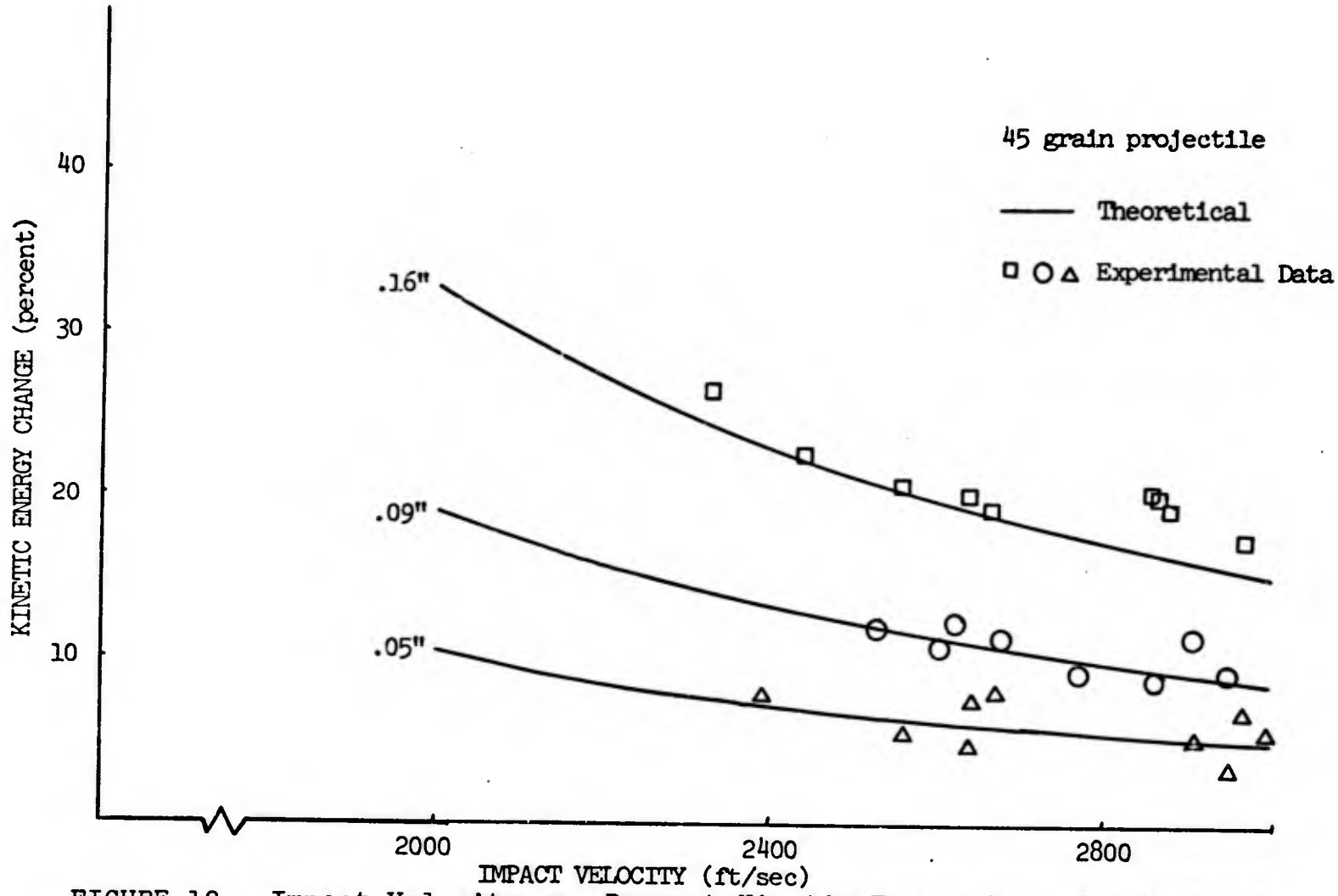


FIGURE 19. Impact Velocity vs. Percent Kinetic Energy Loss for Aluminum Plates of Three Thicknesses

## VI. RECOMMENDATIONS FOR FURTHER STUDY

Experimental studies in the area of hydraulic ram are continuing and further information will be gained. A few specific recommendations are presented as guidelines for future research.

The ballistic range is equipped to fire .30 caliber projectiles. This should be done in order to obtain data for projectiles of higher energies and larger damage radii. In addition, .30 caliber projectiles offer a greater variety of nose shapes which can add information to the previous data on bullet shape effects.

Filled tanks should be penetrated by projectiles of various caliber and mass. This will yield information concerning the effect of fluid foundation on penetration of thin walls.

Finally, it is recommended that the pressure transducers be installed and that experiments be conducted to confirm their effectiveness. If successful, this would give pressures as functions of time for the shock and cavity phases of hydraulic ram, a major step in understanding the phenomenon.

## APPENDIX A

### Explanation of Computer Program

This program computes the distance which a projectile of arbitrary shape and mass will penetrate into a semi-infinite metal plate. Inputs to this program are the shear modulus of the plate material, the mass of the bullet, its maximum radius, and its initial velocity. The cross-sectional area of the bullet at each .032 inch aft of the nose is also read in. Equation (3) is integrated trapezoidally using the bullet area distribution and velocity is tested until it becomes negative. The previous velocity is essentially zero, and the corresponding distance is output as the penetration depth.

```
C  ***********************************************************
C  *                                                         *
C  *   THIS PROGRAM WILL YIELD FOR A GIVEN INITIAL VELOCITY  *
C  *   THE DISTANCE THAT A PROJECTILE OF ARBITRARY AREA      *
C  *   DISTRIBUTION WILL PENETRATE INTO A PLATE OF 7075-T6   *
C  *                        ALUMINUM                         *
C  *                                                         *
C  ***********************************************************
      DIMENSION AREA(3000),AINTEG(3000),X(3000),A(15),
     1DIST(15)
C
CC    READ IN INITIAL DATA
C
      DIST(1)=0.
      RAD=.112
      L=2999
      ALENG=.416
      N=14
      AINTEG(1)=0.
      DELX=1.E-4
      C=15.11E09
      LPL=L+1
      DO 40 I=2,N
   40 DIST(I)=(I-1)*.032
C
CC    READ IN AREA DISTRIBUTION
C
      READ(5,10)(A(J),J=1,N)
   10 FORMAT(8F10.8)
      DO 100 I=1,LPL
      X(I)=DELX*(I-1)
      IF(X(I).GT.ALENG) GO TO 99
      GO TO 88
   99 AREA(I)=3.14159*(RAD**2)
      GO TO 100
C
CC    PIF2 IS AN INTERPOLATION FORMULA
C
   88 AREA(I)=PIF2(X,DIST,N,A,I)
  100 CONTINUE
      K=I
C
CC    READ IN GIVEN IMPACT VELOCITY
C
  400 READ(5,800) VINIT
  800 FORMAT(F8.1)
      IF(VINIT.GT.36000.) GO TO 850
      WRITE(6,300)
  300 FORMAT('0DISTANCE INTO PLATE',12X,'VELOCITY')
      WRITE(6,350) VINIT
  350 FORMAT('0',11X,'0.0',13X,F15.4)
C
CC    NUMERICAL INTEGRATION
C
      DO 600 I=1,K
      AINTEG(I+1)=AINTEG(I)+((AREA(I+1)+AREA(I))/2.)*DELX
      E=VINIT**2-(2.*C*AINTEG(I+1))
      IF(E.LT.0.) GO TO 200
  600 CONTINUE
  200 E=VINIT**2-(2.*C*AINTEG(I))
      VEL=SQRT(E)
      WRITE(6,550) X(I),VEL
  550 FORMAT('0',2X,F15.4,10X,F15.4)
      GO TO 400
  850 STOP
      END
```

```
      FUNCTION PIF2(X,XLIST,N,FLIST,J)
C     SUBPROGRAM FUNCTION 2ND ORDER LOOKUP
      DIMENSION XLIST(200),FLIST(200),X(200)
      BLIF(P,Q,R,S,T)=((Q-P)*(S-T)/(R-Q)+S)
      IF(X(J)-XLIST(N)) 2,1,1
    1 I=N-1
      GO TO 5
    2 IF(X(J)-XLIST(1)) 4,4,6
   10 IF (K-1)  11,11,12
    4 I=1
    5 K=1
      GO TO 30
    6 K=2
    7 DO 8  I=1,N
      IF(X(J)-XLIST(I)) 9,9,8
    8 CONTINUE
      I=N
    9 I=I-1
   30 BLIF1=BLIF(X(J),XLIST(I),XLIST(I+1),FLIST(I),
     1FLIST(I+1))
   11 PIF2 = BLIF1
      RETURN
   12 IF((I+2)-N)  13,13,16
   13 IF((I-1)-1)  15,14,14
   14 IF(ABS(XLIST(I-1)-X(J))-ABS(XLIST(I+2)-X(J))) 16,15,15
   15 L=I+2
      GO TO 17
   16 L=I-1
   17 BLIF2=BLIF(X(J),XLIST(I),XLIST(L),FLIST(I),FLIST(L))
      PIF2=BLIF(X(J),XLIST(I+1),XLIST(L),BLIF1,BLIF2)
   18 RETURN
      END
```

## LIST OF REFERENCES


1. Williams, Roger F., "Shock Effects in Fuel Cells," Stanford Research Institute, Menlo Park, California, October, 1969.

2. Dunn, W. P., "On Material Strengths of the Hypervelocity Impact Problem," AIAA Journal, v. 4, n. 3, p. 535, March, 1966.

3. Margerum, G. W., "A Fiber Optic Pressure Transducer," Aeronautical Engineer Thesis, Naval Postgraduate School, Monterey, California, June, 1972.

4. Yurkovich, R., "Hydraulic Ram: A Fuel Tank Vulnerability Study," McDonnell Douglas Corporation Report No. G964, September, 1969.

5. Lundstrom, E. A., and Stull, E. W., "Fluid Dynamic Analysis of Hydraulic Ram II (Results of Experiments)," Naval Weapons Center, China Lake, California, June, 1973.

6. Menadier, C., Kissinger, C., and Adkins, H., "The Fotonic Sensor," Mechanical Technology, Inc. Bulletin # 02-100.

7. Forman, R. G., Parker, W. H., Gunderson, A. W., Bilek, A., "Vulnerability of Aircraft Structures Exposed to Small Arms Fire Projectile Impact Damage," Air Force Flight Dynamics Laboratory Technical Report AFFDL - TR - 67 - 157, February, 1968.